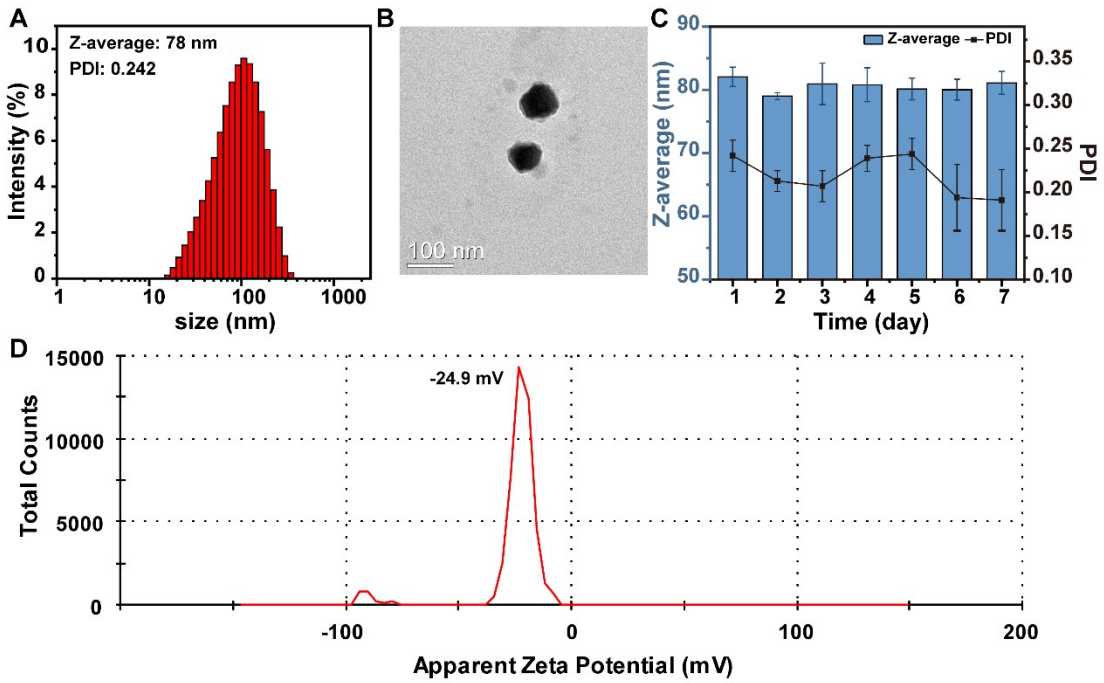

Fig. S1. Characterization of PBDBM NPs. (A) Size distribution of PBDBM NPs. (B) TEM image of PBDBM NPs. (C) Stability of PBDBM NPs. (D) Zeta potential of PBDBM NPs.

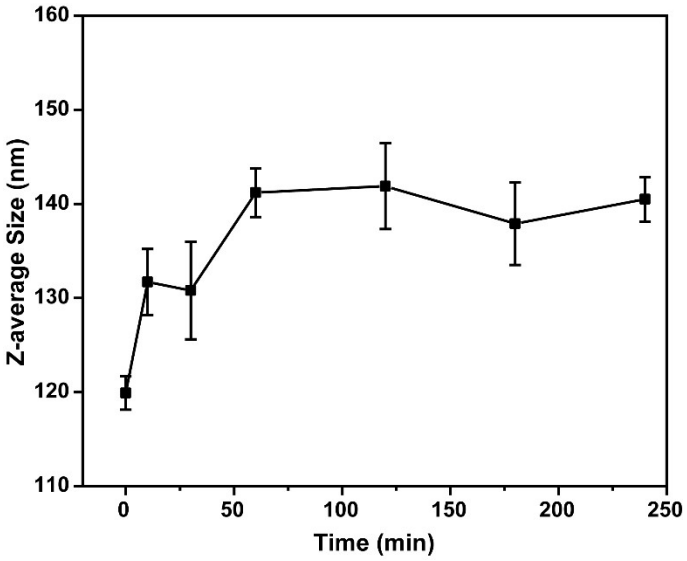

Fig. S2. Z-average size variation of DTX@PBDBM NPs in 10 mM GSH for different times.

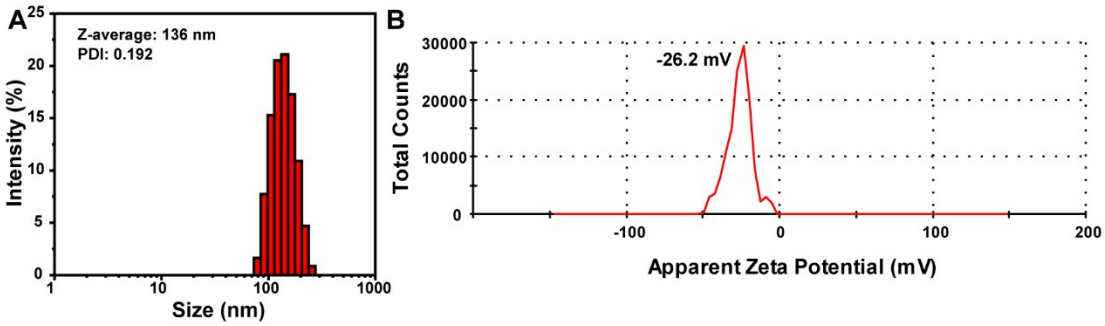

Fig. S3. Characterization of C6@PBDBM NPs. (A) Size distribution of C6@PBDBM NPs. (B) Zeta potential of C6@PBDBM NPs.

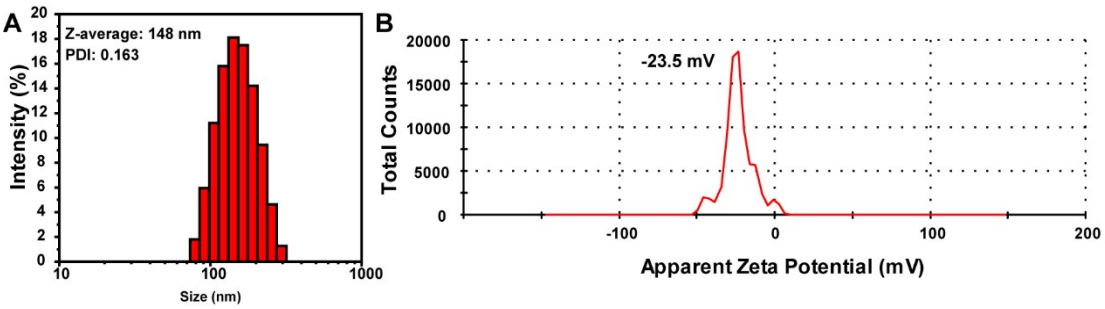

Fig. S4. Characterization of DiR@PBDBM NPs. (A) Size distribution of DiR@PBDBM NPs. (B) Zeta potential of DiR@PBDBM NPs.

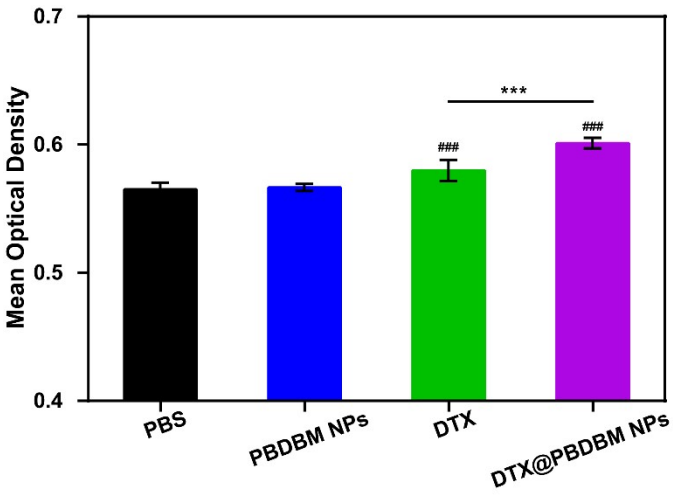

Fig. S5. Mean Optical Density of apoptosis calculated from TUNEL images of tumor sections after systemic administration with PBS, PBDBM NPs, DTX, and DTX@PBDBM NPs. Data were expressed as mean ± S.D. (n = 5). ***$p < 0.001$ vs. DTX group; $^{###}p < 0.001$ vs. PBS group.

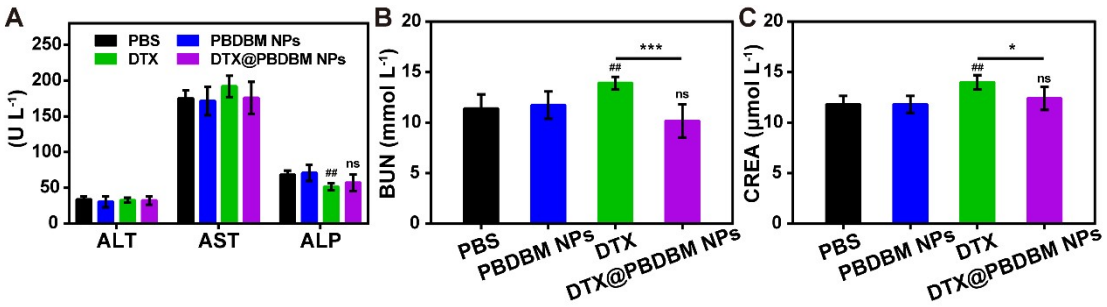

Fig. S6. Blood biochemical analysis of different treatments. (A) ALT, AST, ALP, (B) BUN, (C) CREA level in serum collected from 4T1 tumor-bearing mice after different treatments (n = 5, *p < 0.05, ***p < 0.001 vs. DTX group; $^{\#\#}$p < 0.01 vs. PBS group).

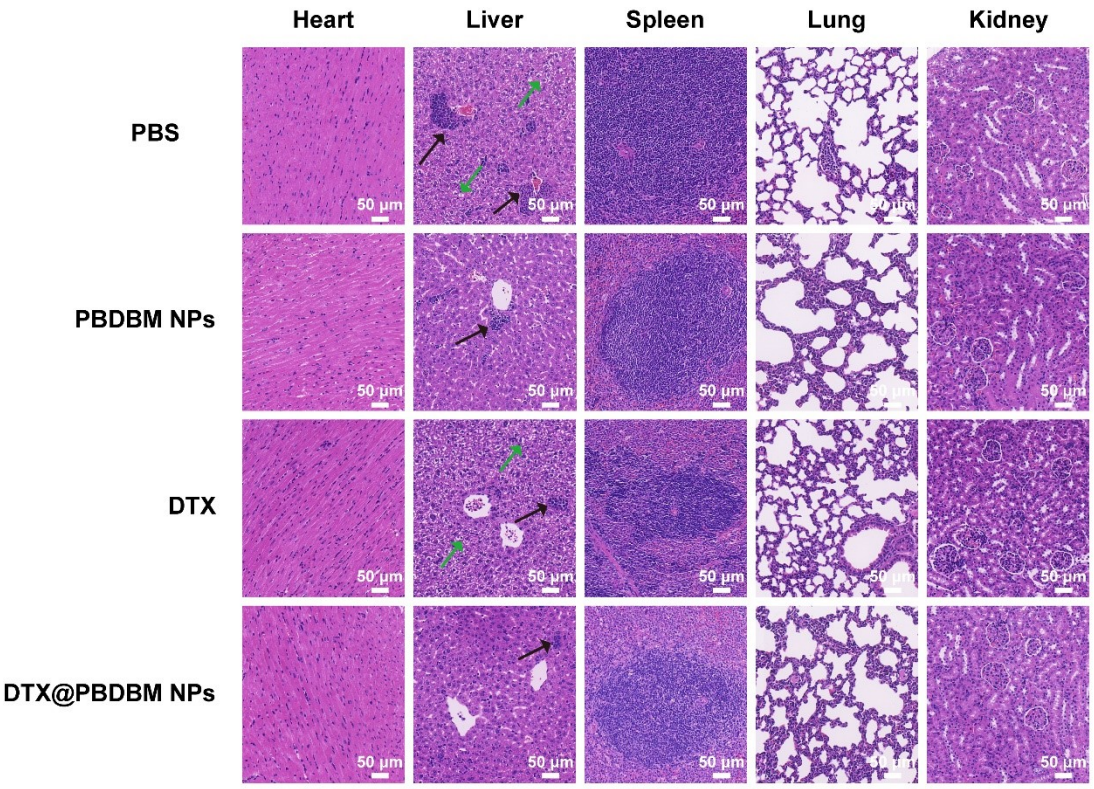

Fig. S7. H&E images of the major organs post systemic treatment with PBS, PBDBM NPs, free DTX, and DTX@PBDBM NPs. Magnification factor: 20×. Scale bar: 50 μm. The black arrows indicate metastatic tumors. The green arrows indicate vacuolar degeneration.